*J. Fluid Mech.* (1979), *vol.* 93, *part* 4, *pp.* 727–736
*Printed in Great Britain*



# Double structures of steady streaming in the oscillatory viscous flow over a wavy wall

By A. KANEKO AND H. HONJI

Research Institute for Applied Mechanics, Kyushu University,
Fukuoka 812, Japan

(Received 11 September 1978)

The steady streaming induced by oscillatory viscous flow of small amplitudes over a wavy wall has been analysed, and the computed flow patterns have been found to agree well with the flow patterns visualized experimentally in a tube. When the first parameter, $L/\delta$ (the ratio of the wavelength of the wavy wall to the thickness of Stokes layer), becomes larger than about 26, the streaming has a double structure consisting of regions of upper and lower pairs of recirculations. As the second parameter, $\alpha/\delta$ (the ratio of the amplitude of the wavy wall to the thickness of Stokes layer), is increased, the upper pair of recirculations squeezes in a gap between the lower recirculations above the troughs of the wall. A similar double structure of steady streamings was also observed above ripple marks formed under oscillatory viscous flow. A bearing is suggested of this phenomenon on the determination of stationary profiles of ripple marks.

## 1. Introduction

The steady streaming induced by oscillatory flow over a wavy wall has been an important subject in the study of the formation of ripple marks under water waves (Uda & Hino 1975; Sleath 1976; Kaneko & Honji 1978). The oscillatory flow over a wavy wall is very complicated since two representative length scales, the wavelength and the wave height of the wall, are concerned. Lyne (1971) studied the steady streaming over a wavy wall and suggested that the streaming has diverse structures depending on the profile of a wall and other flow conditions. For both the amplitude of oscillation and the thickness of the Stokes layer much smaller than the wall wavelength, the streaming acquires double structures, of which the vertical scale is nearly equal to the wavelength.

In this paper, an attempt is made to extend Lyne's theory by considering higher-order solutions of a similar perturbation scheme. This enables us to obtain different double structures of the streaming, which are in agreement with the results of flow visualization experiments in a tube. In §§ 2 and 3 respectively, the methods of analysis and experimental procedures are described. In § 4, the experimental results obtained by means of a rigid wavy wall are presented in parallel with those of analysis. Some experimental results on the formation of ripple marks under oscillatory viscous flow are also presented in § 5.

0022–1120/79/4295–7170 $02.00 

## 2. Analysis

Let us consider the vorticity equation for two-dimensional oscillatory flow over an infinite wavy wall. We shall make use of rectangular cartesian co-ordinates $(x, y)$, with $x$ measured parallel to the mean level of the wall and $y$ measured normal to it. Let $t$ denote time and $\Psi$ a stream function. We introduce the following non-dimensional quantities,

$$\left.\begin{aligned} \psi &= \Psi/U_\infty \delta, \quad \xi = x/L, \quad \eta = y/\delta, \\ \tau &= \omega t, \quad \epsilon = 2a/L, \quad \delta = (2\nu/\omega)^{\frac{1}{2}}, \end{aligned}\right\} \tag{1}$$

where $\delta$ is the thickness of the Stokes layer, $L$ the wall wavelength, and $\nu$ the kinematic viscosity of a fluid. The quantities $U_\infty$, $\omega$ and $a$ are the maximum flow velocity, the angular frequency, and the amplitude of fluid oscillation at $\eta = \infty$, respectively. The basic equation in a non-dimensional form is

$$2\frac{\partial}{\partial\tau}(D^2\psi) - \epsilon\frac{\partial(\psi, D^2\psi)}{\partial(\xi,\eta)} = D^2(D^2\psi), \tag{2}$$

where

$$D^2 = \frac{\partial^2}{\partial\eta^2} + \left(\frac{\delta}{L}\right)^2\frac{\partial^2}{\partial\xi^2}.$$

A profile of the wall is given by

$$\eta_0 = \frac{\alpha}{\delta}\cos 2\pi\xi, \tag{3}$$

where $\alpha$ is the amplitude of the wall. The boundary conditions for (2) may be assumed here to be

$$\begin{aligned} &\psi = \partial\psi/\partial\eta = 0 \quad \text{on} \quad \eta = \eta_0, \\ &\partial\psi/\partial\eta \to \cos\tau \quad \text{as} \quad \eta \to \infty. \end{aligned} \tag{4}$$

Let us consider only the case $\epsilon \ll 1$ and look for a perturbation solution for (2) of a form

$$\psi = \psi_0 + \epsilon\psi_1 + \epsilon^2\psi_2 + \ldots. \tag{5}$$

Substituting (5) into (2) and equating like powers of $\epsilon$, we obtain the equation

$$2\frac{\partial}{\partial\tau}(D^2\psi_0) = D^2(D^2\psi_0) \tag{6}$$

for $\epsilon^0$.

We expand the solution of (6), $\psi_0$, in a form

$$\psi_0 = \mathscr{R}\left[e^{i\tau}\sum_{n=0}^{\infty} f_n(\eta)\cos 2n\pi\xi\right], \tag{7}$$

where $\mathscr{R}$ denotes 'real part of'. Substituting (7) into (6) and eliminating the summation symbol from the resulting equation, we obtain

$$\frac{d^4 f_n}{d\eta^4} - 2[(nk\delta)^2 + i]\frac{d^2 f_n}{d\eta^2} + (nk\delta)^2[(nk\delta)^2 + 2i]f_n = 0 \quad \text{for} \quad n = 0, 1, 2, \ldots, \tag{8}$$

where the wavenumber $k = 2\pi/L$. Taking into account the boundary conditions as $\eta \to \infty$ in (4), we obtain the solutions for (8),

$$\begin{aligned} f_0 &= \eta + a_0 + b_0\exp[-(1+i)\eta] \quad \text{for} \quad n = 0, \\ f_n &= a_n\exp(-\sigma_n\eta) + b_n\exp(-nk\delta\eta) \quad \text{for} \quad n \geqslant 1, \end{aligned} \tag{9}$$

where $\sigma_n^2 = (nk\delta)^2 + 2i$. Since we consider the case $\alpha/\delta \ll 1$, like Lyne, the boundary conditions for $\eta = \eta_0$ in (4) may be expanded in the Taylor series at $\eta = 0$. In (9), $f_0$ corresponds to the Stokes shear-wave solution for a flat wall and is of order

$(\alpha/\delta)^0$. Equating like harmonic terms of $\xi$ in the expansion and considering the order of $f_0$, we can estimate $f_n$ as

$$f_n \sim O[(\alpha/\delta)^n] \quad \text{for} \quad n \geqslant 1. \tag{10}$$

By neglecting the terms of orders higher than $(\alpha/\delta)^2$, for example, two boundary conditions on $\eta = \eta_0$ become:

$$\left.\begin{aligned} f_0 + \frac{1}{2}\frac{\alpha}{\delta}\frac{df_1}{d\eta} + \frac{1}{4}\left(\frac{\alpha}{\delta}\right)^2 \frac{d^2 f_0}{d\eta^2} &= 0, \\ f_1 + \frac{\alpha}{\delta}\frac{df_0}{d\eta} &= 0 \end{aligned}\right\} \tag{11}$$

and

$$f_2 + \frac{1}{2}\frac{\alpha}{\delta}\frac{df_1}{d\eta} + \frac{1}{4}\left(\frac{\alpha}{\delta}\right)^2 \frac{d^2 f_0}{d\eta^2} = 0;$$

and

$$\left.\begin{aligned} \frac{df_0}{d\eta} + \frac{1}{2}\frac{\alpha}{\delta}\frac{d^2 f_1}{d\eta^2} + \frac{1}{4}\left(\frac{\alpha}{\delta}\right)^2 \frac{d^3 f_0}{d\eta^3} &= 0, \\ \frac{df_1}{d\eta} + \frac{\alpha}{\delta}\frac{d^2 f_0}{d\eta^2} &= 0 \end{aligned}\right\} \tag{12}$$

and

$$\frac{df_2}{d\eta} + \frac{1}{2}\frac{\alpha}{\delta}\frac{d^2 f_1}{d\eta^2} + \frac{1}{4}\left(\frac{\alpha}{\delta}\right)^2 \frac{d^3 f_0}{d\eta^3} = 0.$$

When orders up to $(\alpha/\delta)^{n_0}$ are considered, the corresponding boundary conditions are given by means of similar procedures. We can thus determine the unknown coefficients for $f_n (n = 0, 1, 2, \ldots, n_0)$ from these boundary conditions.

Let us consider the terms of order $\epsilon^1$ in (2); we obtain

$$\left(2\frac{\partial}{\partial\tau} - D^2\right) D^2\psi_1 = \frac{\partial(\psi_0, D^2\psi_0)}{\partial(\xi, \eta)}. \tag{13}$$

Substituting (7) into the right-hand side of (13), we see that $\psi_1$ may be written as the sum of a term independent of $\tau$ and a term depending on $\tau$ as $e^{2i\tau}$. Attention is now focused on the term independent of $\tau$. We put the steady part of $\psi_1$ into $\psi_s$ and write

$$\psi_s = f_s + f_s^*, \tag{14}$$

where the asterisk denotes 'complex conjugate'. When the orders up to $(\alpha/\delta)^{n_0}$ are considered, the equation for $f_s$ becomes

$$\begin{aligned} D^2(D^2 f_s) = &-\frac{\pi}{2}\sum_{n=1}^{n_0} n\left[\frac{df_0^*}{d\eta}\left\{\frac{d^2 f_n}{d\eta^2} - (nk\delta)^2 f_n\right\} - f_n\frac{d^3 f_0^*}{d\eta^3}\right]\sin 2n\pi\xi \\ &-\frac{\pi}{4}\sum_{n=1}^{n_0}\sum_{m=1}^{n}(n-m)\left[\frac{df_m^*}{d\eta}\left\{\frac{d^2 f_{n-m}}{d\eta^2} - (n-m)^2(k\delta)^2 f_{n-m}\right\}\right. \\ &\left.-f_{n-m}\left\{\frac{d^3 f_m^*}{d\eta^3} - (mk\delta)^2\frac{df_m^*}{d\eta}\right\}\right]\sin 2n\pi\xi \\ &-\frac{\pi}{4}\sum_{n=1}^{n_0-2}\sum_{m=1}^{[\frac{1}{2}(n_0-n)]}(m+n)\left[\frac{df_m^*}{d\eta}\left\{\frac{d^2 f_{m+n}}{d\eta^2} - (m+n)^2(k\delta)^2 f_{m+n}\right\}\right. \\ &\left.-f_{m+n}\left\{\frac{d^3 f_m^*}{d\eta^3} - (mk\delta)^2\frac{df_m^*}{d\eta}\right\}\right]\sin 2n\pi\xi \\ &+\frac{\pi}{4}\sum_{n=1}^{n_0-2}\sum_{m=1}^{[\frac{1}{2}(n_0-n)]} m\left[\frac{df_{m+n}^*}{d\eta}\left\{\frac{d^2 f_m}{d\eta^2} - (mk\delta)^2 f_m\right\}\right. \\ &\left.-f_m\left\{\frac{d^3 f_{m+n}^*}{d\eta^3} - (m+n)^2(k\delta)^2\frac{df_{m+n}^*}{d\eta}\right\}\right]\sin 2n\pi\xi, \end{aligned} \tag{15}$$

where [ ] on the summation symbols indicates that the largest possible integer should be taken.

We now look for a solution of (15) of the form

$$f_s = \sum_{n=1}^{n_0} g_n(\eta) \sin 2n\pi\xi, \tag{16}$$

where $g_n \sim O[(\alpha/\delta)^n]$. Substituting (9) and (16) into (15), we obtain the equation

$$\begin{aligned}\left[\frac{d^2}{d\eta^2} - (nk\delta)^2\right]^2 g_n = &-n\pi i[a_n \exp(-\sigma_n\eta) - 2(1-i)a_n b_0^* \exp\{-(\sigma_n+1-i)\eta\} \\ &-(1-i)b_n b_0^* \exp\{-(nk\delta+1-i)\eta\}] \\ &+\frac{\pi i}{2}\sum_{m=1}^{n}(n-m)[\sigma_m^* a_m^* b_{n-m} \exp\{-[\sigma_m^*+(n-m)k\delta]\eta\} \\ &+2\sigma_m^* a_m^* a_{n-m} \exp\{-(\sigma_m^*+\sigma_{n-m})\eta\} \\ &+mk\delta b_m^* a_{n-m} \exp\{-(\sigma_{n-m}+mk\delta)\eta\}] \\ &+\frac{\pi i}{2}\sum_{m=1}^{[\frac{1}{2}(n_0-n)]}(m+n)[\sigma_m^* a_m^* b_{m+n} \exp[-\{\sigma_m^*+(m+n)k\delta\}\eta] \\ &+2\sigma_m^* a_m^* a_{m+n} \exp\{-(\sigma_m^*+\sigma_{m+n})\eta\} \\ &+mk\delta a_{m+n} b_m^* \exp -(\sigma_{m+n}+mk\delta)\eta\}] \\ &-\frac{\pi i}{2}\sum_{m=1}^{[\frac{1}{2}(n_0-n)]} m[\sigma_{m+n}^* a_{m+n}^* b_m \exp\{-(\sigma_{m+n}^*+mk\delta)\eta\} \\ &+2\sigma_{m+n}^* a_{m+n}^* a_m \exp\{-(\sigma_m+\sigma_{m+n}^*)\eta\} \\ &+(m+n)k\delta a_m b_{m+n}^* \exp\{-[\sigma_m+(m+n)k\delta]\eta\}]\end{aligned} \tag{17}$$

for $g_n$ $(n = 1, 2, \ldots, n_0)$, where the last two terms of the right-hand side of (17) disappear for $n \geqslant n_0 - 1$. The boundary conditions for (17) become

$$\left.\begin{aligned} g_n = 0, \quad \frac{dg_n}{d\eta} = 0 \quad \text{at} \quad \eta = 0, \\ \frac{dg_n}{d\eta} \to 0 \quad \text{as} \quad \eta \to \infty, \end{aligned}\right\} \tag{18}$$

for $n = 1, 2, \ldots, n_0$. The solutions $g_n$ $(n = 1, 2, \ldots, n_0)$ for (17) are given by

$$\begin{aligned} g_n = &A_n^{(1)} \exp(-\sigma_n\eta) + A_n^{(2)} \exp[-(\sigma_n+1-i)\eta] + A_n^{(3)} \exp[-(nk\delta+1-i)\eta] \\ &+(A_n^{(4)} + A_n^{(5)}\eta)\exp(-nk\delta\eta) \\ &+\sum_{m=1}^{n}[B_{mn}^{(1)} \exp\{-[\sigma_m^*+(n-m)k\delta]\eta\} + B_{mn}^{(2)} \exp\{-(\sigma_m^*+\sigma_{n-m})\eta\} \\ &+B_{mn}^{(3)} \exp\{-(\sigma_{n-m}+mk\delta)\eta\}] \\ &+\sum_{m=1}^{[\frac{1}{2}(n_0-n)]}[B_{mn}^{(4)} \exp\{-[\sigma_m^*+(m+n)k\delta]\eta\} + B_{mn}^{(5)} \exp\{-(\sigma_m^*+\sigma_{m+n})\eta\} \\ &+B_{mn}^{(6)} \exp\{-(\sigma_{m+n}+mk\delta)\eta\} \\ &+B_{mn}^{(7)} \exp\{-(\sigma_{m+n}^*+mk\delta)\eta\} + B_{mn}^{(8)} \exp\{-(\sigma_m+\sigma_{m+n}^*)\eta\} \\ &+B_{mn}^{(9)} \exp\{-[\sigma_m+(m+n)k\delta]\eta\}], \end{aligned} \tag{19}$$

where the coefficients in (19) are to be determined from (17) and (18). The solution $g_1$ almost coincides with Lyne's solution obtained by making use of orthogonal curvilinear co-ordinates.

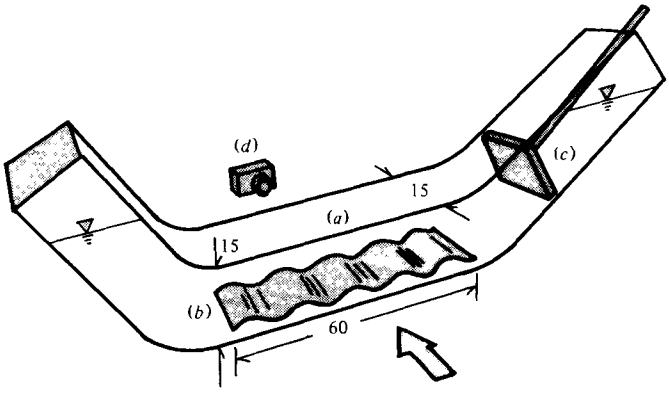


FIGURE 1. Schematic diagram of experimental set-up (dimensions in cm). The arrow indicates the direction of light projection. (*a*) Test section, (*b*) wavy wall, (*c*) piston, (*d*) camera.

Considering the terms of order $\epsilon^2$ in (2), we obtain

$$\left(2\frac{\partial}{\partial\tau}-D^2\right)D^2\psi_2=\frac{\partial(\psi_0,D^2\psi_1)}{\partial(\xi,\eta)}+\frac{\partial(\psi_1,D^2\psi_0)}{\partial(\xi,\eta)}. \tag{20}$$

Since the terms independent of $\tau$ do not appear in the right-hand side of (20), $\psi_2$ has no steady part. Therefore, the stream function $\psi_s$ can be written from (14) and (16) as

$$\psi_s=\sum_{n=1}^{n_0}G_n(\eta)\sin 2n\pi\xi+O\left\{\left(\frac{\alpha}{\delta}\right)^{n_0+1},\epsilon^3\right\}, \tag{21}$$

where $G_n(\eta)=g_n(\eta)+g_n^*(\eta)$. The non-dimensional wall shear stress ($\tau_s$) induced by steady streamings can be written as

$$\tau_s=\sum_{n=1}^{n_0}\frac{d^2G_n(0)}{d\eta^2}\sin 2n\pi\xi+O\left\{\left(\frac{\alpha}{\delta}\right)^{n_0+1},\epsilon^3\right\}. \tag{22}$$

When the values of parameters $L/\delta(=2\pi/k\delta)$ and $\alpha/\delta$ are given, we can determine numerically the streamlines and the wall shear stress for steady streamings by (21) and (22), respectively. The results computed up to the order of $(\alpha/\delta)^7$ are given in § 4.

## 3. Experimental methods

The experiment was carried out with a U-shaped rectangular tube illustrated in figure 1. A test section of the tube made of a transparent plastic plate is $15\times15$ cm in cross-section and 60 cm in length. In order to reduce flow disturbances, two corners of the tube are curved smoothly. A fluid in the test section was oscillated by a motor-driven piston. The maximum period and the maximum amplitude of fluid oscillation were 1·1 s and 5·5 cm, respectively. Three wavy walls made of a thin aluminium plate were used as test walls, of which wavelengths were 4, 8, and 12 cm. One of the walls was placed on the bottom floor of the tube. The amplitude of fluid oscillation was 0·6 cm. The profile of the walls was approximately sinusoidal. The wave height was 0·3 cm, and the values of the steepness were therefore 1/13·3, 1/26·7, and 1/40·0. In the experiments on the formation of ripple marks, a layer of glass beads 1 cm thick replaced the test walls. The mean diameter of glass beads was 0·028 cm.

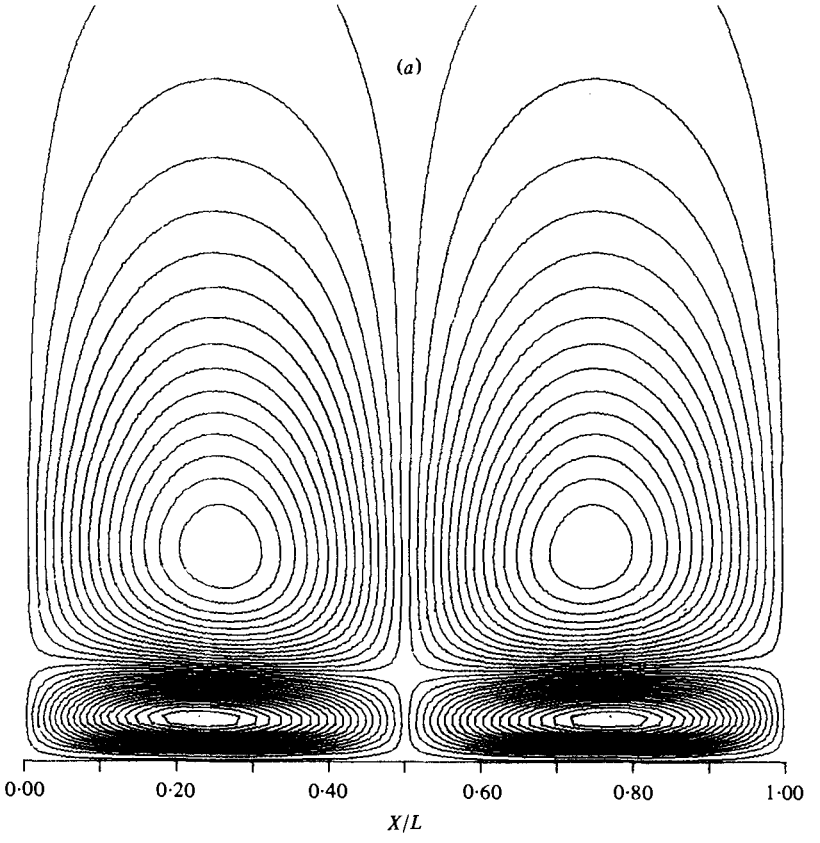


FIGURE 4 (*a*). For the legend see p. 733.

All the experiments were carried out using glycerin–water solutions with $\nu$ ranging from 0·81 to 1·20 $cm^2 s^{-1}$. A slight optical inhomogeneity of the solutions was used to visualize the flow pattern of steady streamings. This direct shadow method was initiated by Hagerty & Mich (1950), and applied recently to visualize the steady streaming over a wavy wall by Hino & Fujisaki (1977). The test section filled with the fluid was projected through a first side wall by a nearly parallel beam of intense light, and the resulting shadows on a white paper put on the back of a second side wall were photographed by a 35 mm camera.

## 4. Flows over rigid wavy walls

As described in § 2, streamlines for steady streaming over wavy walls have been computed numerically. The streamlines are plotted over one wavelength ranging from crest to crest; the horizontal unit scale is $L$ and the vertical one is $\delta$ in all the computed figures. Two neighbouring streamlines in each figure have the same differences in the value of $\psi_s$.

Figure 2 (*a*) (plate 1) shows the computed streamlines at $L/\delta = 7{\cdot}3$ and $\alpha/\delta = 0{\cdot}27$. When $L/\delta$ is as small as the value for figure 2 (*a*), the steady streaming forms a pair of recirculations having a vertical scale comparable to the wavelength and rotating

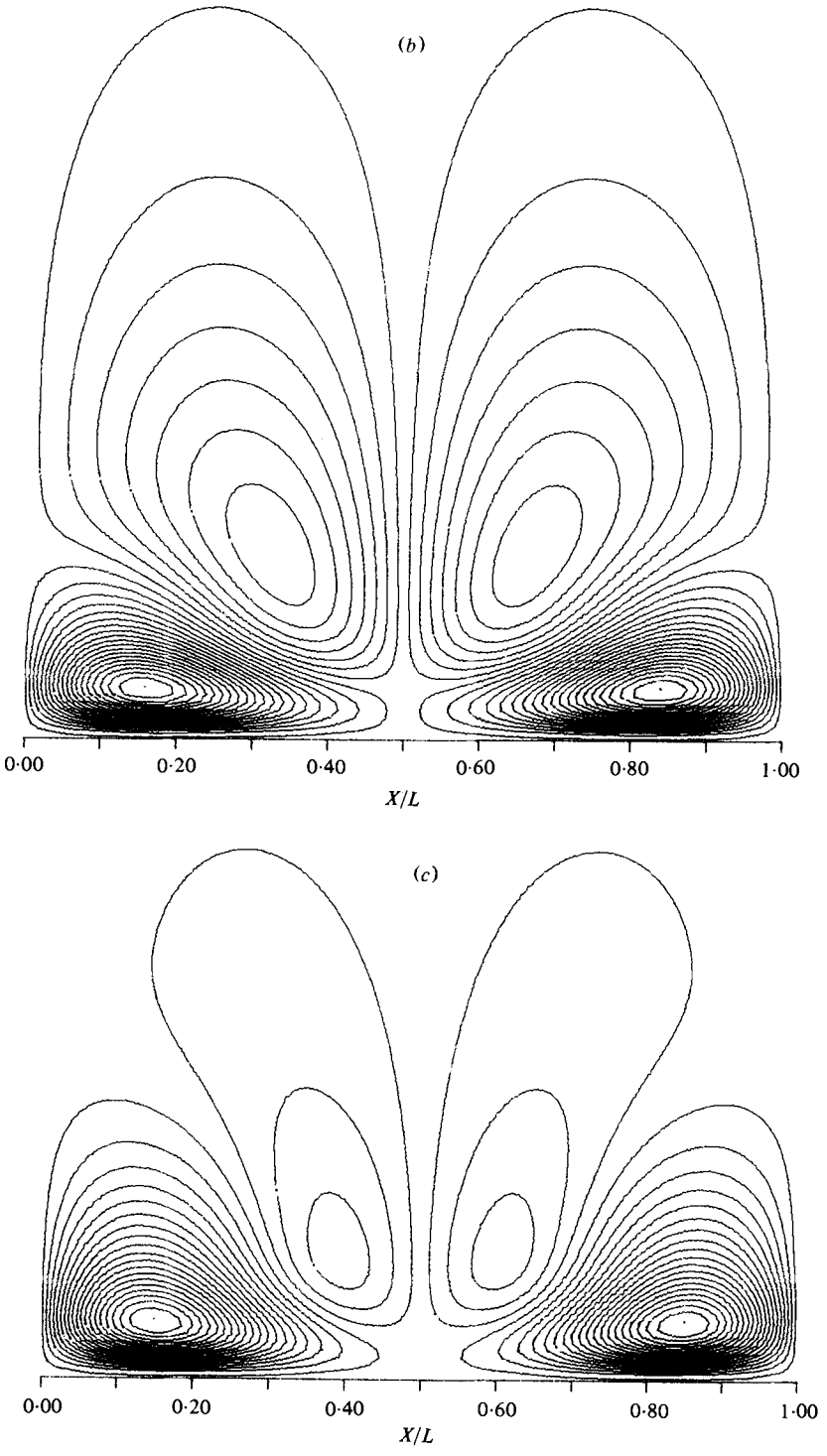


FIGURE 4. Computed flow patterns at $L/\delta = 39$.
(*a*) $\alpha/\delta = 0{\cdot}05$, (*b*) $\alpha/\delta = 0{\cdot}47$, (*c*) $\alpha/\delta = 0{\cdot}7$.

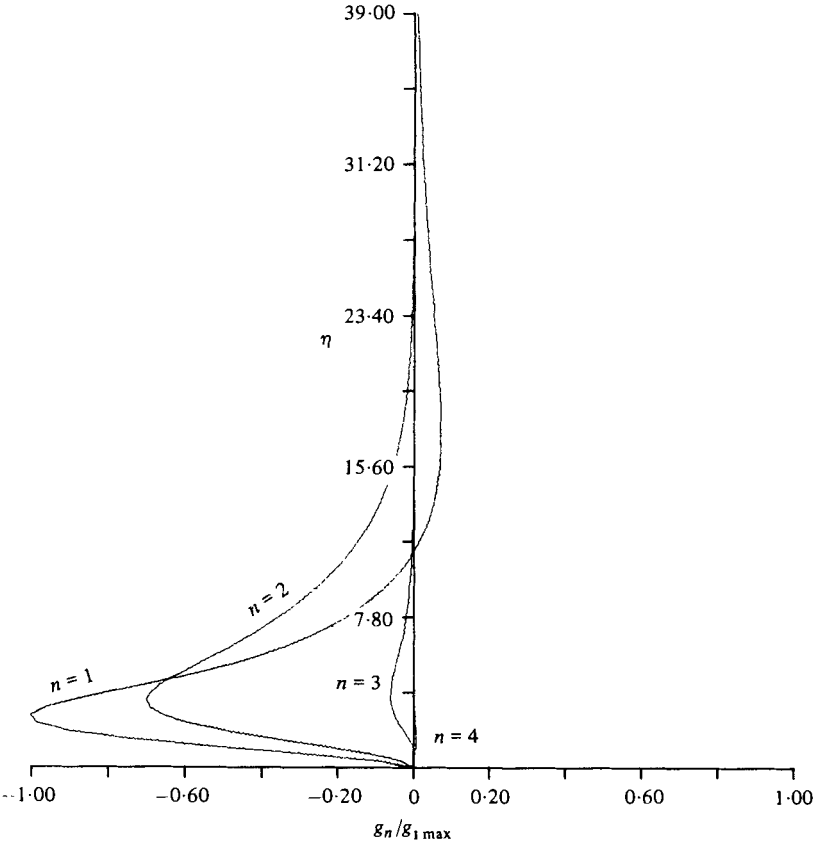


FIGURE 5. Profiles of $g_n$ ($n = 1, 2, 3, 4$).

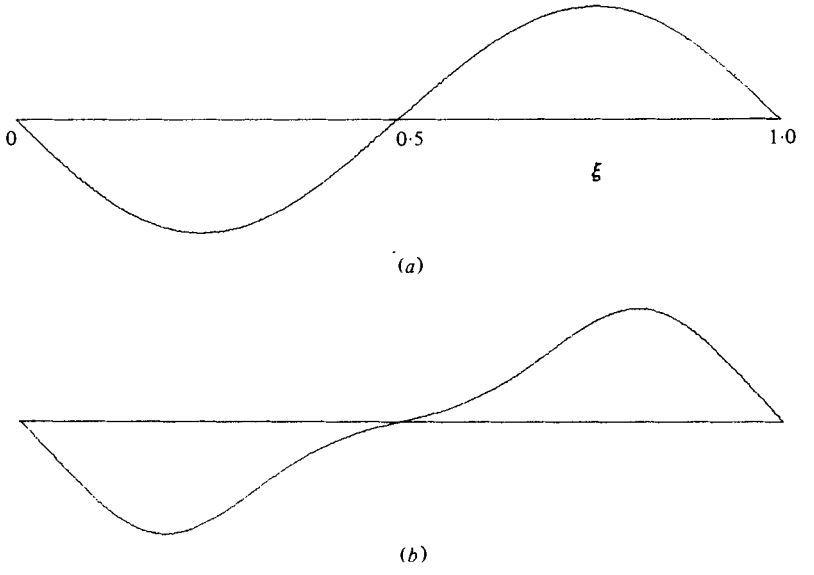


FIGURE 6. Distributions of wall shear stress: (*a*) for figure 4(*a*) and (*b*) for figure 4(*c*).

| | $2a$ (cm) | $\omega$ (rad s$^{-1}$) | $\nu$ (cm$^2$ s$^{-1}$) | $\delta$ (cm) | $L$ (cm) | $\alpha$ (cm) | $2a/L(=\epsilon)$ | $L/\delta$ | $\alpha/\delta$ |
|---|---|---|---|---|---|---|---|---|---|
| Experiment 1 | 5·5 | 9·6 | 1·20 | 0·50 | 9 | 0·3 | 0·61 | 18·0 | 0·60 |
| Experiment 2 | 11·0 | 6·0 | 1·20 | 0·63 | 10 | 0·4 | 1·10 | 15·9 | 0·63 |

TABLE 1. Data for flows over ripple marks.

in such a direction that the flow along the bottom surface goes up the slopes of the wall. It should be noted that this direction of the flow is evidently favourable in making up ripple marks. Figure 2(*b*) shows a flow pattern visualized under the same flow conditions as those for figure 2(*a*). Although the steady streaming began to develop immediately after the fluid oscillation had started, it took more than 5 minutes to reach the stationary state. All the presented pictures are of a stationary state. Agreement between figures 2(*a*, *b*) is good, when observing the position of vortex centres and the vertical scale of the regions of recirculations.

Figure 3(*a*) (plate 2) shows the computed flow pattern at $L/\delta = 28$ and $\alpha/\delta = 0{\cdot}47$. When $L/\delta$ is increased, the recirculation regions are flattened in shape and a new pair of recirculation regions appears above the former ones. The flow direction of the upper recirculation is opposite to that of the lower one. Such a double structure of steady streamings appears at a critical value of $L/\delta = 26$. This critical condition is almost independent of $\alpha/\delta$. Figure 3(*b*) shows a visualized flow pattern with the flow conditions nearly equal to those for figure 3(*a*). A pair of upper weak recirculations is also formed above the trough of the wavy wall.

Figure 4 shows a series of the computed streamline patterns for a large value of $L/\delta\,(=39)$. When $\alpha/\delta$ is small, the flow pattern almost coincides with those of Lyne as shown in figure 4(*a*). As $\alpha/\delta$ is increased, $g_n\,(n \geqslant 2)$ neglected in Lyne's analysis affects the structure of steady streamings, and the upper pair of recirculations squeezes in a gap between the lower recirculations as shown in figure 4(*b*). At present, no process of determination of $L$ is known for real ripple marks. There seems to be a possibility that squeezing of the upper recirculations may serve as a clue in understanding the process. Figure 4(*c*) shows the computed flow pattern for a large value of $\alpha/\delta\,(=0{\cdot}7)$. The upper recirculations are reduced in intensity, and their vortex centres approach to the wall surface appreciably.

Figure 5 shows profiles of $g_n\,(n = 1, 2, 3, 4)$ computed under the same conditions as figure 4(*c*). Each value of $g_n$ is normalized by the maximum value of $g_1$. It is seen from the figure that, when $\alpha/\delta$ is as large as the value concerned here, $g_2$ has a magnitude comparable to that of $g_1$ and must be retained in the determination of flow patterns. It is seen also that the effect of $g_n\,(n \geqslant 3)$ on the flow pattern may decrease rapidly.

The distributions of $\tau_s$ for both cases of figures 4(*a*, *c*) are shown in figure 6, in which $\tau_s$ is normalized by its maximum value. As $\alpha/\delta$ is increased, the slope of the curve decreases gradually at a trough. However, figure 6 indicates that the upper pair of recirculations is not in touch with the wall surface.

Figure 7(*a*) (plate 3) shows a visualized flow pattern in conditions similar to those for figure 4(*b*). The upper region of recirculations is developed over the lower ones as has been predicted by the theory. The flow pattern around a trough is shown in a magnified scale in figure 7(*b*). The bottom of the upper recirculations looks as if it

were rooted to the wall trough by pushing aside the lower recirculations. This seems to support the aforementioned possibility that squeezing of the upper recirculations may affect the formation of real ripple marks.

## 5. Flows over ripple marks

It has been found that ripple marks are formed under oscillatory viscous flow by using glycerin–water solutions as a working fluid. Two kinds of experiments were carried out at different values of $2a/\delta$, which corresponds to the Reynolds number for oscillatory viscous flow over a flat wall. The experimental data are given in table 1.

Figure 8 (plate 4) shows an instantaneous pattern of steady streamings over the stationary ripple marks, at $2a/\delta = 11{\cdot}0$ and at the values of other parameters shown in experiment 1. When a stationary profile of ripple marks was reached, the steady streaming became to have a regular double structure consisting of the regions of upper and lower pairs of recirculations. The bottom of the upper recirculations pushing aside the lower ones approached the surface of ripple marks. No separation region is seen in figure 8.

Figure 9 (plate 4) shows a flow pattern at $2a/\delta = 17{\cdot}5$ and at the values of parameters shown in experiment 2. As $2a/\delta$ is increased, clear streamlines of the lower recirculations disappear and the flow begins to separate from the crests. Experiments 1 and 2 show that the double structures of steady streamings appear at $L/\delta = 18{\cdot}0$ and $15{\cdot}9$, respectively. These values of $L/\delta$ are smaller than 26 predicted in § 4. These differences may be due to the effect of increasing $\epsilon$ on the structure of steady streamings in figures 8 and 9.

## 6. Conclusions

Streamline patterns of the steady streaming induced by the oscillatory viscous flow over a rigid wavy wall have been computed and compared with flow patterns obtained by means of the direct shadow method. Agreement between the theory and the observations for overall flow patterns has been satisfactory. Streamings over the ripple marks have also been observed.

The results are as follows. (1) The steady streaming has a double structure consisting of the upper and lower regions of recirculations, when $L/\delta > 26$ approximately. The appearance of the double structure is almost independent of $\alpha/\delta$. (2) As $\alpha/\delta$ is increased, the upper pair of recirculations squeezes in a gap between the lower recirculations at the trough. (3) The ripple marks are formed under oscillatory viscous flow. When ripple marks become stationary, the streamline patterns become to have a double structure.

The authors wish to thank Prof. J. Okabe, Prof. M. Takematsu, and Dr M. Oikawa for valuable discussions. The authors also wish to thank Y. Shiraishi, N. Matsunaga, and M. Kamachi for technical assistance.

REFERENCES

HAGERTY, W. W. & MICH, A. A. 1950 *J. Appl. Mech.* **17**, 54–58.
HINO, M. & FUJISAKI, H. 1977 *Proc. Int. Symp. on Flow Visualisation*, Tokyo, pp. 229–234.
KANEKO, A. & HONJI, H. 1979 *Sedimentology* **26**, 101–113.
LYNE, W. H. 1971 *J. Fluid Mech.* **50**, 33–48.
SLEATH, J. F. A. 1976 *J. Hydraul. Res.* **14**, 69–81.
UDA, T. & HINO, M. 1975 *Proc. Japan Soc. Civil Engng* **237**, 27–36.

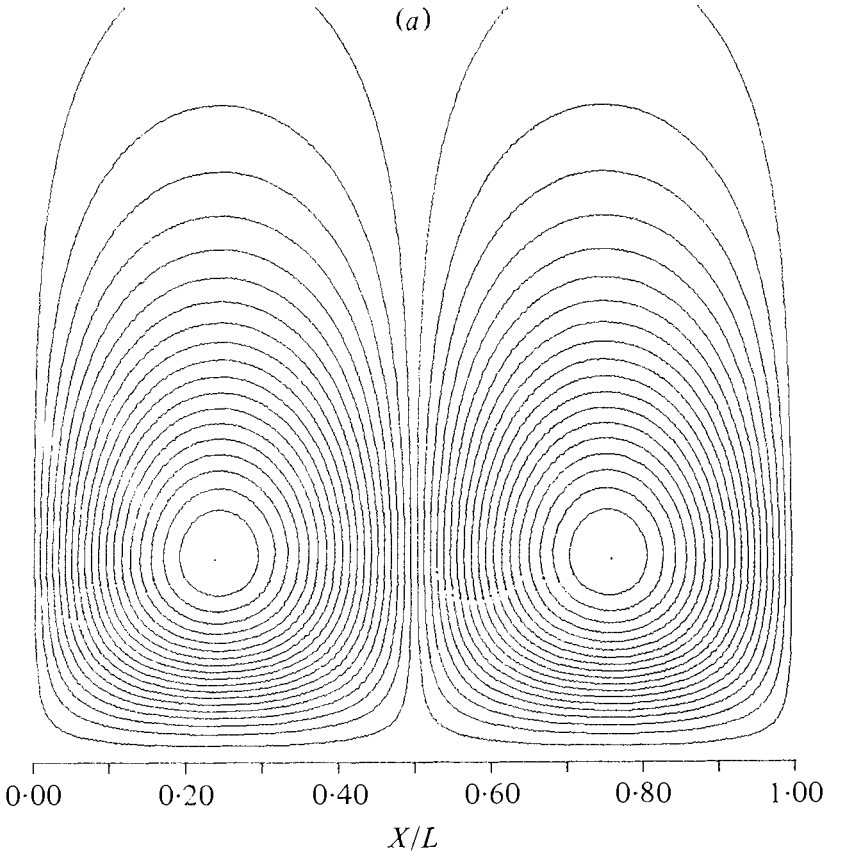


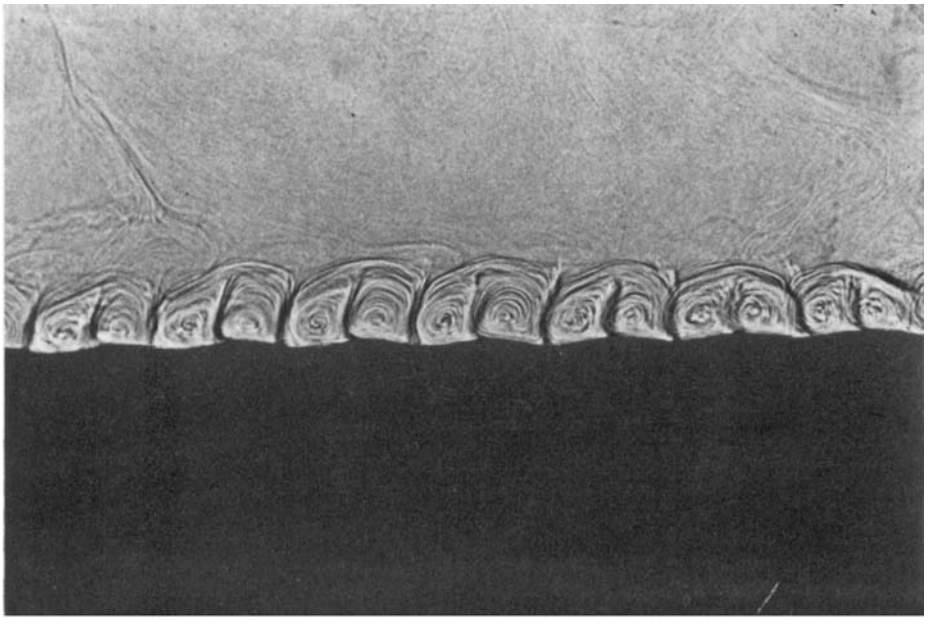

(b)

FIGURE 2. Flow patterns at $L/\delta = 7{\cdot}3$ and $\alpha/\delta = 0{\cdot}27$. (*a*) Computed flow pattern, (*b*) observed flow pattern; $L = 4$ cm, $\alpha = 0{\cdot}15$ cm, $\nu = 1{\cdot}01$ cm$^2$ s$^{-1}$, and $\delta = 0{\cdot}55$ cm.

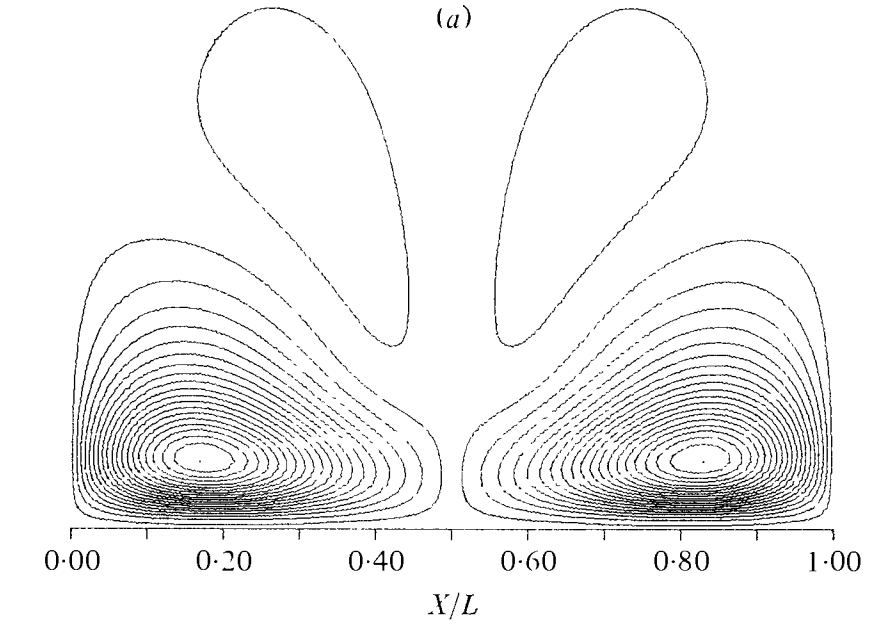


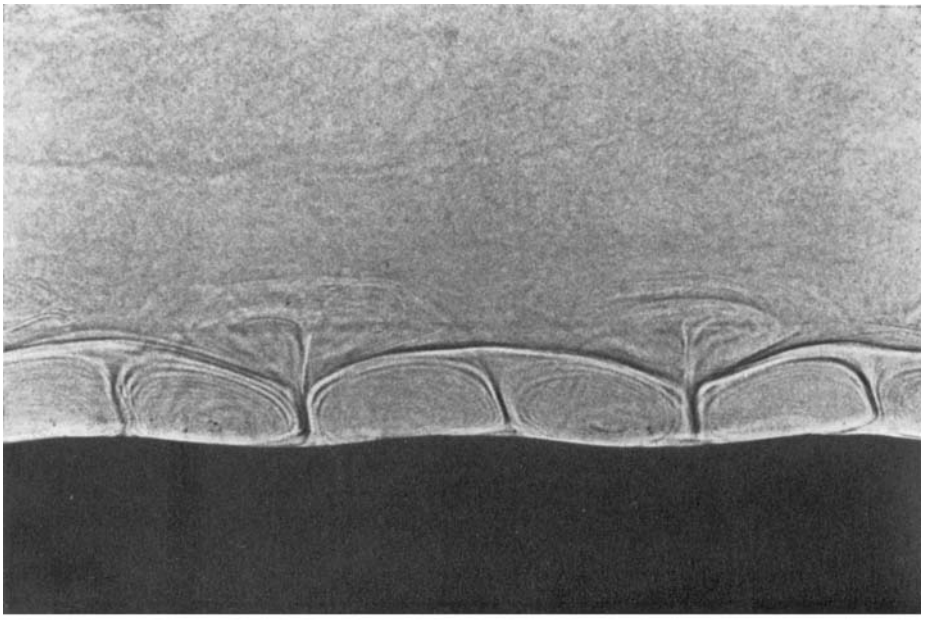

(b)

FIGURE 3. Flow patterns at a initiation stage of upper recirculation regions. (*a*) Computed flow pattern; $L/\delta = 28$ and $\alpha/\delta = 0{\cdot}47$. (*b*) Observed flow pattern; $L/\delta = 24$, $\alpha/\delta = 0{\cdot}46$. $L = 8$ cm, $\alpha = 0{\cdot}15$ cm, $\nu = 0{\cdot}86\,\mathrm{cm^2\,s^{-1}}$, and $\delta = 0{\cdot}33$ cm.

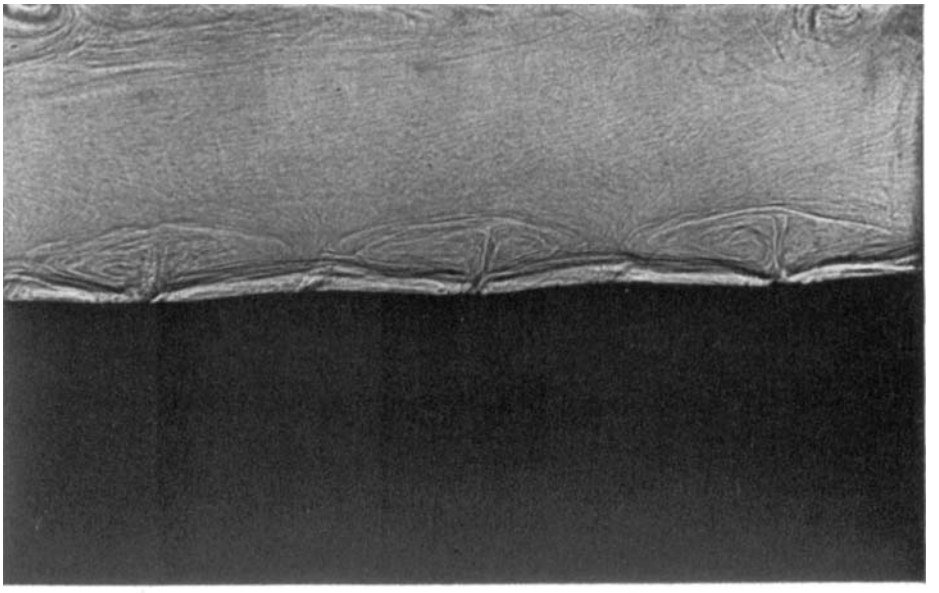

(*a*)

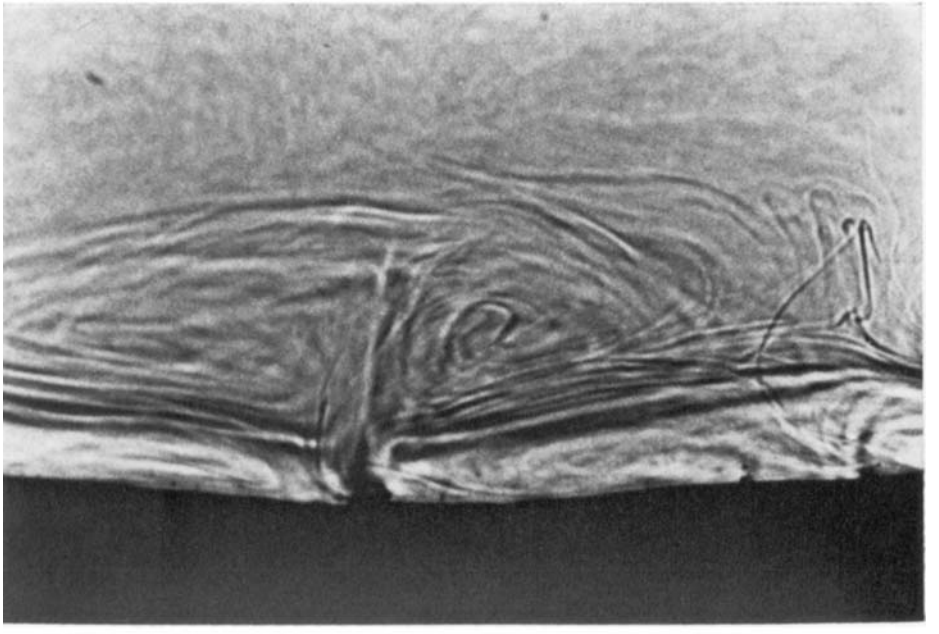

(*b*)

FIGURE 7. Flow patterns at $L/\delta = 39$ and $\alpha/\delta = 0{\cdot}47$; $L = 12$ cm, $\alpha = 0{\cdot}15$ cm, $\nu = 0{\cdot}81$ cm$^2$ s$^{-1}$, and $\delta = 0{\cdot}32$ cm. (*a*) Distant view; (*b*) near view.

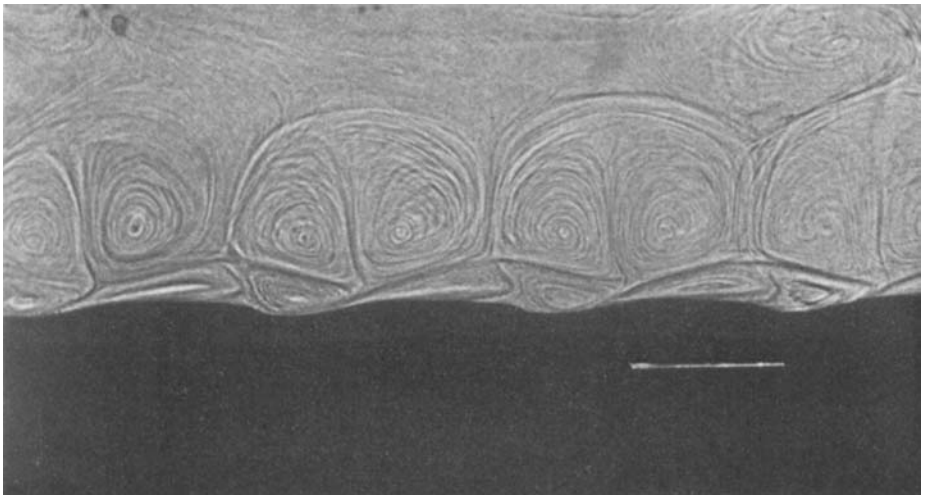

FIGURE 8. Flow patterns over ripple marks at $2a/\delta = 11{\cdot}0$.

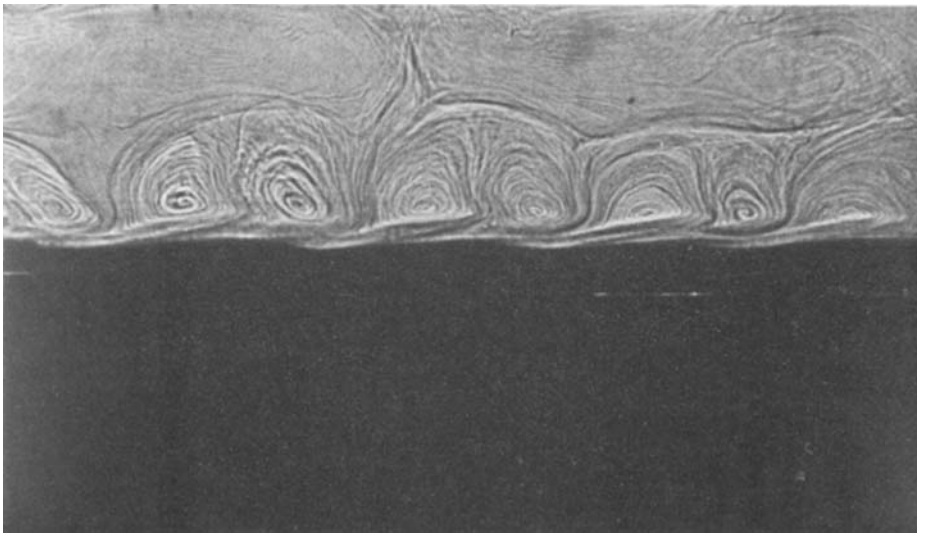

FIGURE 9. Flow patterns over ripple marks at $2a/\delta = 17{\cdot}5$.